CHEMISTRY OF MATERIALS
Article

Chem. Mater. **2010,** *22,* 5401–5410 5401
DOI:10.1021/cm101438x

Alternative Approach to Increasing Li Mobility in Li-La-Nb/Ta Garnet Electrolytes

May Nyman,* Todd M. Alam, Sarah K. McIntyre, Grant C. Bleier, and David Ingersoll

Sandia National Laboratories, P.O. Box 5800 MS-0754 Albuquerque, New Mexico 87185

Received January 4, 2010. Revised Manuscript Received August 23, 2010

The solid-state lithium electrolytes $Li_5La_3Ta_2O_{12}$ and $Li_5La_3Nb_2O_{12}$ have been the focus of recent studies due to their chemically robust nature (against the lithium electrode; particularly the tantalate analogue) and high lithium conductivity. Structural characterization and Li-conductivity studies have shown that there are two populations of lithium cations, nominally called octahedral (less tightly bound) and tetrahedral sites (tightly bound), and the octahedrally coordinated lithium are considerably more mobile than the tetrahedrally coordinated lithium. In this study, we have documented two methods to preferentially vacate the tetrahedral or nonmobile lithium sites. This is accomplished by either Li_2O volatility upon repeated mixing and heating solid-state processing steps or by aqueous $H^+ \rightarrow Li^+$ exchange, followed by removal of the exchanged-in H^+ by water vaporization. The aqueous treatment produces the largest change in the tetrahedral (nonmobile) lithium sites concentration. The ability to ion-exchange the Li^+ also suggests an aqueous instability of these phases that is not widely recognized. These processes are documented by ^{6}Li MAS NMR, infrared spectroscopy, and thermogravimetry. Combined ^{6}Li and ^{7}Li NMR studies show that aqueous treatment significantly increases the dynamics of the remaining Li sites. The NMR energy of activation (E_a) for lithium mobility in $Li_{5-x}La_3Ta_2O_{12-x/2}$ decreases by ~54% for the long-T_1 Li component and ~14% for the fast-T_1 component following heat treatment, while subsequent aqueous treatment revealed a slow component with a similar E_a to the heat treated sample but with the short-T_1 component showing an approximate doubling in the E_a.

Introduction

Lithium-ion solid-state electrolytes with the garnet structure have been studied extensively for potential use in electrochemical applications such as solid-state batteries.[1] A variety of compositional variations have been investigated including $Li_{3+x}Nd_3Te_{2-x}Sb_xO_{12}$,[2] $Li_7La_3Zr_2O_{12}$,[3] $Li_7La_3Sn_2O_{12}$,[4] and $Li_5La_3M_2O_{12}$ (M = Nb, Ta).[5−11] Additional derivatives of $Li_5La_3M_2O_{12}$ include alkaline-earth (AE) substituted $Li_{5+x}AE_xLa_{3-x}M_2O_{12}$ (M = Nb, Ta; AE = Sr, Ba),[4,6,7,12] and $Li_{5.5}La_3Nb_{1.75}In_{0.25}O_{12}$ and $Li_{5.5}La_{2.75}K_{0.25}Nb_2O_{12}$.[13] In particular, the composition $Li_5La_3Ta_2O_{12}$ has noteworthy electrochemical and chemical stability in contact with the lithium electrode,[8] and the composition $Li_6BaLa_2Ta_2O_{12}$ exhibits the best conductivity of 4×10^{-5} S/cm at room temperature.[14] A motivating factor of many of these composition-variation studies is to increase the Li-population, predominantly by incorporating lower valence metals on the 8-coordinate and the 6-coordinate sites of the garnet framework. By this strategy; as lithium population increases, it first occupies tetrahedral sites, which are face-sharing with vacant octahedral sites. With continued increase in the Li-population, the octahedral sites become populated, forcing lithium off the tetrahedral sites due to Li−Li repulsion (Li−Li face-sharing distance ~2.0 Å).[15] Since the lithium on the tetrahedral sites is relatively nonmobile and the lithium on the octahedral sites is mobile, the tandem increase in the $Li_{octahedral}$ and decrease in the $Li_{tetrahedral}$ results in increased Li-mobility.[2]

While this approach has proven fruitful, especially in the case of $Li_6BaLa_2Ta_2O_{12}$,[14] a somewhat contrary strategy of decreasing the overall Li-population also seems promising, in that opening up the pathways for Li-mobility should decrease the activation energy for site-hopping. In this study, we have explored the possibility of taking advantage

*Corresponding author. E-mail: mdnyman@sandia.gov.

(1) Knauth, P. *Solid State Ionics* **2009**, *180*, 911–916.
(2) O'Callaghan, M. P.; Powell, A. S.; Titman, J. J.; Chen, G. Z.; Cussen, E. J. *Chem. Mater.* **2008**, *20*, 2360–2369.
(3) Awaka, J.; Kijima, N.; Hayakawa, H.; Akimoto, J. *J. Solid State Chem.* **2009**, *182*, 2046–2052.
(4) Percival, J.; Slater, P. R. *Solid State Commun.* **2007**, *142*, 355–357.
(5) Cussen, E. J. *Chem. Commun.* **2006**, 412–413.
(6) Murugan, R.; Thangadurai, V.; Weppner, W. *Appl. Phys. A: Mater. Sci. Process.* **2008**, *91*, 615–620.
(7) Murugan, R.; Thangadurai, V.; Weppner, W. *J. Electrochem. Soc.* **2008**, *155*, A90–A101.
(8) Thangadurai, V.; Adams, S.; Weppner, W. *Chem. Mater.* **2004**, *16*, 2998–3006.
(9) Thangadurai, V.; Kaack, H.; Weppner, W. J. F. *J. Am. Ceram. Soc.* **2003**, *86*, 437–440.
(10) vanWullen, L.; Echelmeyer, T.; Meyer, H. W.; Wilmer, D. *Phys. Chem. Chem. Phys.* **2007**, *9*, 3298–3303.
(11) Mazza, D. *Mater. Lett.* **1988**, *7*, 205–207.
(12) Awaka, J.; Kijima, N.; Takahashi, Y.; Hayakawa, H.; Akimoto, J. *Solid State Ionics* **2009**, *180*, 602–606.
(13) Thangadurai, V.; Weppner, W. *J. Solid State Chem.* **2006**, *179*, 974–984.
(14) Thangadurai, V.; Weppner, W. *Adv. Funct. Mater.* **2005**, *15*, 107.
(15) O'Callaghan, M. P.; Cussen, E. J. *Chem. Commun.* **2007**, 2048–2050.

Published on Web 09/07/2010

of Li_2O volatility (vaporizes readily at 600 °C) to introduce both Li^+ and corresponding O^{2-} vacancies in $Li_5La_3M_2O_{12}$ (M = Nb, Ta) and probe the effect on Li-mobility, utilizing ^6Li and ^7Li magic-angle spinning (MAS) NMR spectroscopies. While ^6Li NMR provided a means of identifying and quantifying different Li-populations, ^7Li NMR spin−lattice relaxation studies provided information on lithium mobility as a function of population density. Furthermore, through a combination of extensive powder processing and heating studies and ion-exchange studies, in corroboration with NMR experiments on the garnet phases, we were able to identify a distinct Fourier transform infrared (FTIR) spectroscopy fingerprint for the nonmobile lithium population. This provided a rapid and easy method for following the process of depopulation of lithium, either by extensive heating and processing or by aqueous ion-exchange of lithium for protons. Finally, the ease of $H^+ \rightarrow Li^+$ exchange followed by conversion to a Li-poor phase illustrates the possible instability of these garnet electrolyte phases in the presence of moisture that is not widely recognized.

Experimental Section

Synthesis of $Li_5La_3Nb_2O_{12}$ and $Li_5La_3Ta_2O_{12}$. Our synthesis of the garnet phases was adapted from the previously reported procedure.[8] In a typical reaction, 10 g of lanthanum nitrate hexahydrate (23 mmol $La(NO_3)_3 \cdot 6H_2O$), 3.89 g of Ta_2O_5 or 2.34 g of Nb_2O_5 (15.3 mmol), and 2 g of $LiOH \cdot H_2O$ (38.3 mmol) are placed in a 60 mL plastic tube with ∼30 YSZ milling beads and 20 mL of isopropanol. The tube is capped tightly and sealed with electrical tape and mixed on a Turbula System Schatz WAB (Basel, Switzerland) for 20−60 min. The resulting slurry is thick and homogeneous, resembling white paint. The slurry is poured into a ceramic crucible, filtering out the shaking beads. The crucible is then placed in a vacuum oven at ∼40 °C overnight. Note: at this step, the slurry never completely dries, probably due to the hygroscopic nature of the lanthanum nitrate. The crucible containing the precursor mixture is then heated in a box furnace at 700 °C for 6−12 h. This step results in decomposition of the nitrate salt. In the second processing step, the powder is then remixed with ∼0.4 g of $LiOH \cdot H_2O$ and placed in a 900 °C furnace overnight. At this step, the powder product is nearly pure garnet phase, as determined by powder X-ray diffraction, and is white in color.

Extensive Processing of $Li_5La_3Nb_2O_{12}$ and $Li_5La_3Ta_2O_{12}$. The tantalate garnet obtained as described above is designated LiLaTa-white in the following characterization experiments. To obtain garnet samples with more extensive processing and heating, we simply repeated the second step of the procedure described above (add 0.4 g of lithium hydroxide to the powder, remix, and heat at 900 °C overnight). For both the niobate and tantalate analogues, the tantalate in particular, the color of the powder changed from white to pink with ∼3−5 reprocessing steps. These samples are designated LiLaTa-pink and LiLaNb-pink. As a final step, the powders are again reprocessed with lithium hydroxide and heated for 4 days at 900 °C. These were designated LiLaTa-tan and LiLaNb-tan, in that the color deepened to a tan hue. In our syntheses, we never observed a LiLaNb powder that was completely white, it always appeared off-white in color.

$H^+ \rightarrow Li^+$ Exchange of Garnet Phases. When a powder sample of either $Li_5La_3Nb_2O_{12}$ or $Li_5La_3Ta_2O_{12}$ is placed in water in a beaker and stirred, the pH rises to around 10−11 (depending on the concentration of the powder). This is due to exchange of H^+ from the aqueous media, which displaces Li^+ from the garnet lattice. For a neutral $H^+ \rightarrow Li^+$ exchange, the powder is stirred for 30 min at room temperature and then recollected by vacuum filtration. For a pH∼3 $H^+ \rightarrow Li^+$ exchange, while stirring at room temperature, we add dropwise a 1 M HNO_3 solution, while monitoring the pH. When the pH reaches 2.5−3, the solution is left stirring for another hour. The pH rises to ∼3.5 during this time. The $H^+ \rightarrow Li^+$ exchanged garnet powder is then recollected by vacuum filtration.

Characterization of Garnet Samples. Powder X-ray diffraction was carried out on a Bruker D8 Advance diffractometer in Bragg−Brentano geometry with Cu−Kα radiation and a diffracted-beam graphite monochromator. Infrared spectra (400−4000 cm^{-1}) were recorded on a Thermo Nicolet 380 FT-IR equipped with a Smart Orbit (Diamond) ATR accessory. Thermal analysis was executed with a TA Instruments SDT 2960 for simultaneous thermogravimetric and differential thermal analysis (TGA-DTA) under air flow with a heating rate of 10 °C/min. Samples for compositional analysis (wt % Li) were submitted to Galbraith Laboratories, Inc. (Knoxville, TN).

NMR Studies. The solid state ^6Li and ^7Li NMR were obtained on a Bruker Avance 400 instrument at 58.89 and 155.52 MHz, respectively. Both the static and MAS spectra were obtained using a 4 mm broadband MAS probe, spinning at 10 kHz. The ^6Li MAS spectra were obtained using a single pulse Bloch decay with a 600 s recycle delay, 128−256 scan averages, while the ^7Li MAS spectra only required 32 scan averages using a $\pi/12$ pulse (0.5 μs) and a 10 s recycle delay. The $^1H-^6Li$ CPMAS NMR experiments were performed using a standard CP sequence, a 40 s recycle delay with contact times ranging from 10 μs to 5 ms. The sample temperature under MAS conditions was calibrated using the ^{207}Pb chemical shift variation of a secondary external $Pb(NO_3)_2$ standard and therefore corrected for increases in sample temperature resulting from spinning.[16,17] The wide-line static ^7Li NMR spectra were obtained using a Hahn echo, with a 400 ns dwell and 32 scan averages. The variable temperature (VT) static and MAS NMR experiments were controlled to ±1 °C in accuracy. Both the $^{6,7}Li$ chemical shifts were referenced to a sealed 1 M LiCl secondary chemical shift reference (δ = 0 ppm). Simulations of the observed static NMR lineshapes (overlapping broad and narrow components) and the first order quadrupolar MAS NMR line shapes were obtained using DMFIT.[18] The ^7Li spin−lattice relaxation rates ($R_1 = 1/T_1$) were obtained using a saturation recovery with 16 different time increments. The signal intensities in the relaxation recovery experiments were fit to a bimodal decay to account for the different relaxation behavior of the central and satellite transitions using ref 23

$$S(t) = S_0(1 - \{A \exp[-(t/T_1{}^A)^{\beta_A}] + (1-A)\exp[-(t/T_1{}^B)^{\beta_B}]\})$$

For the current discussion, the stretch parameters were fixed to $\beta_A = \beta_B = 1$ to reduce the number of variables. The limited relaxation curves were fit reasonably well using this biexponential decay.

(16) Bielecki, A.; Burum, D. P. *J. Magn. Reson., Ser. A* **1995**, *116*, 215–220.
(17) Takahashi, T.; Kawashima, H.; Sugisawa, H.; Baba, T. *Solid State Nucl. Magn. Reson.* **1999**, *15*, 119.
(18) Massiot, D.; Fayon, F.; Capron, M.; King, I.; Le Calve, S.; Alonso, B.; Durand, J.-O.; Bujoli, B.; Gan, Z.; Hoatson, G. *Magn. Reson. Chem.* **2002**, *40*, 70–76.

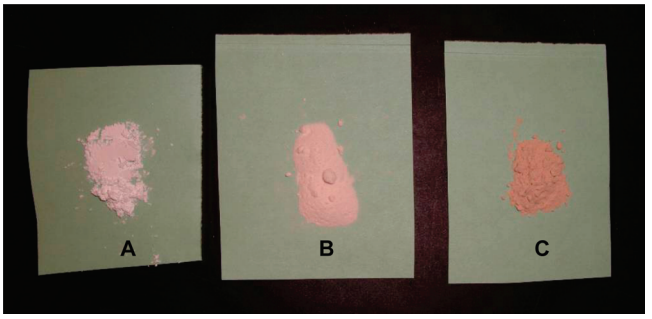

Figure 1. Powders of $Li_5La_3Ta_2O_{12}$ (LiLaTa), showing the color change as a function of increasing number of processing steps. (A) LiLaTa-white, (B) LiLaTa-pink, and (C) LiLaTa-tan.

Results and Discussion

Synthesis. A curious feature of the garnet phase, both for Ta and Nb analogues but more apparent in the Ta analogue, is the color as a function of increased number of processing steps and/or heating time. After a few heating steps, the powders take on a pinkish hue. Extensive heating (for multiple days) produced a tan-colored material. Three examples are shown in Figure 1 for the Ta analogue. We have also observed this same color transformation in the solid-state synthesis and processing of Li_3TaO_4. This is not a function of an impurity phase, since we do not identify any by X-ray diffraction: the diffraction patterns of white, pink, and tan samples appear virtually identical. We do not observe any impurity elements by scanning electron energy-dispersive spectroscopy (SEM-EDS). Furthermore, if the color came from an impurity such as iron or manganese, we would observe the color in the precursors as well. We are not certain of the origin of this color, but it may be correlated to the formation of Li and/or oxygen vacancies, per the following discussions. A "darkening" of lithium niobate and lithium tantalate has been described prior, attributed to reduction of Ta/Nb^{5+} to Ta/Nb^{4+}, with a corresponding oxygen-vacancy formation,[19,20] so this may also be a possibility. Typical X-ray diffraction patterns for the $Li_5La_3Ta_2O_{12}$ and $Li_5La_3Nb_2O_{12}$ powders are shown in Figure 2. The powders are essentially phase-pure garnet: the peaks match those of the JCPDF patterns for the respective phases.

In every publication describing the synthesis of this family of garnet phases, the synthesis protocol was essentially the same. The salient features include (1) ball-milling or mixing with mortar and pestle (often in isopropanol), (2) the first heating step is carried out as a powder, (3) any subsequent heating steps were carried out in a pellet form, usually with 10−20% excess lithium and usually with the pellet covered with powder of the same stoichiometry. In our general synthetic procedures, we had two distinct differences: (1) we utilize a Turbula, a high powered shaker, to remix our powders at every stage of processing, and (2) in general, our powders were not pressed into pellets for any heating steps. Both of these processing parameters have the potential for increasing lithium volatility. The Turbula produces very fine powders, increasing the surface area from which the lithium can vaporize. Furthermore, pelletizing a powder should also diminish surface area and consequently reduce lithium volatility.

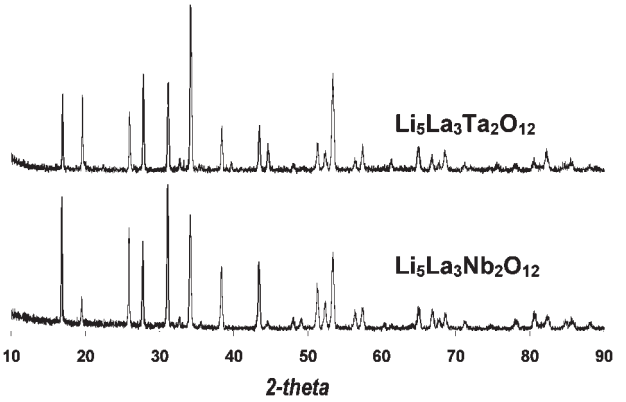

Figure 2. Typical X-ray powder diffraction spectra of $Li_5La_3Ta_2O_{12}$ (top) and $Li_5La_3Nb_2O_{12}$ (bottom).

Each remixing and reheating step required addition of excess LiOH, otherwise partial conversion to the related Li-poorer La_2LiTaO_6 phase occurred. This is inconsistent with the report by O'Callaghan and Cussen,[21] where five 12 h heating steps (in the pellet form) were carried out to synthesize $Li_6SrLa_2Ta_2O_{12}$ without resulting in excess Li loss or conversion to a Li-poorer phase. The difference may be the effect of the Turbula or pellet processing conditions, but also likely the Sr-substitution stabilizes the oxide lattice against alteration.

NMR Characterization. *^{7}Li NMR.* Figure 3 (left) shows the static ^{7}Li NMR for both the LiLaTa samples (white, pink, and tan) and the LiLaNb samples (pink, tan). These multicomponent NMR spectra result from the superposition of narrow and broad Gaussians produced by the central ($^1/_2 \leftrightarrow -^1/_2$) and satellite transitions ($\pm^1/_2 \leftrightarrow \pm^3/_2$), respectively. These broad lines are characteristic of spin $I = {}^3/_2$ systems where the distinct features of the quadrupolar powder patterns (horns and edges) are not observed due to broadening produced by distributions in the electrical field gradient (EFG) tensor and homo- and heteronuclear dipolar coupling.[22] For the tantalate garnet materials, the full width at half-maximum (fwhm) of the central transition varied slightly between 5520 and 5750 Hz for the different processing methods, while for the Nb garnet materials the fwhm ranged from 6180 to 6430 Hz.

The ^{7}Li MAS NMR spectra (10 kHz spinning speed) for the LiLaTa and LiLaNb materials samples are shown in Figure 3 (right) and reveal a set of spinning sidebands arising from the satellite transition produced by a quadrupolar coupling constant (QCC) ∼ 100 kHz (also consistent with the QCC obtained from the static ^{7}Li NMR spectra). The MAS removed inhomogenous broadening

(19) DeLeo, G. G.; Dobson, J. L.; Masters, M. F.; Bonjack, L. H. *Phys. Rev. B* **1988**, *37*, 8394–8400.
(20) Kappers, L. A.; Sweeney, K. L.; Halliburton, L. E. *Phys. Rev. B* **1985**, *31*, 6792–6794.
(21) O'Callaghan, M. P.; Cussen, E. J. *Solid State Sci.* **2008**, *10*, 390–395.
(22) Bohmer, R.; Jeffrey, K. R.; Vogel, M. *Prog. Nucl. Magn. Reson. Spectrosc.* **2007**, *50*, 87–174.
(23) Koch, B.; Vogel, M. *Solid State Nucl. Magn. Reson.* **2008**, *34*, 37–43.

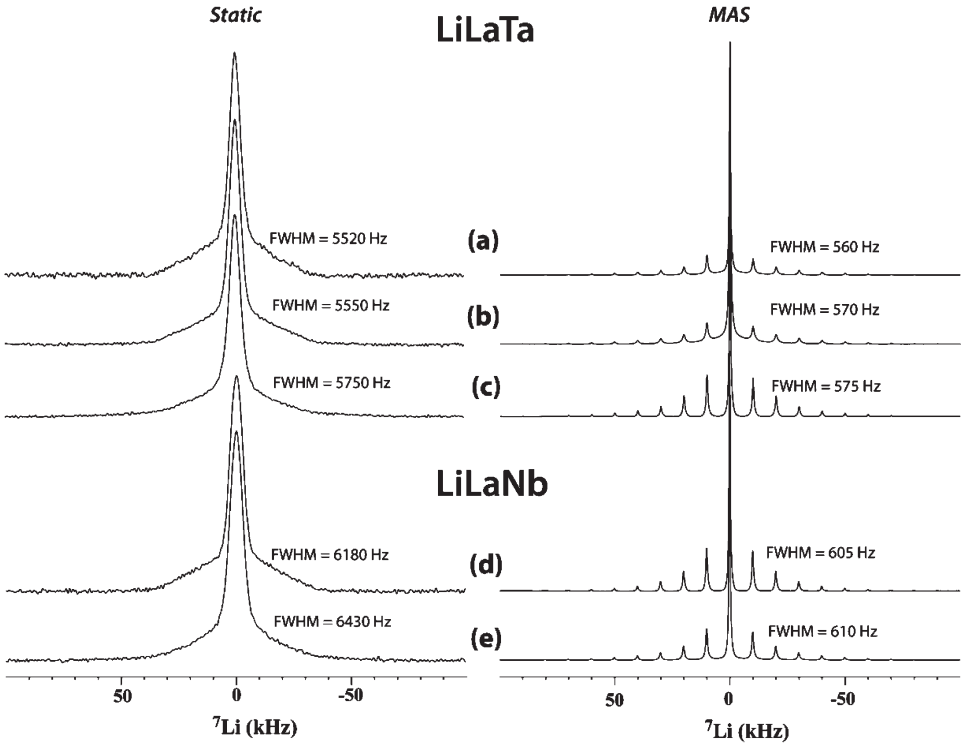

Figure 3. The ^{7}Li static (left) and MAS (right) NMR spectra for the LiLaTa garnet materials (a) white, (b) pink, and (c) tan and the LiLaNb garnet materials (d) pink and (e) tan.

and reduces the central transition fwhm by a factor of ~10. In the case of ^{7}Li, the central transition is still broadened by homonuclear ^{7}Li dipolar coupling and is responsible for the ^{7}Li MAS fwhm line widths being larger than line widths observed in the ^{6}Li MAS NMR (see below). The differences in the static and MAS fwhm between the LiLaTa and the LiLaNb materials shows increased dipolar coupling in the Nb series and reflects either an increase in ^{7}Li homonuclear coupling or the presence of a stronger ^{7}Li−^{93}Nb heteronuclear coupling. The ^{181}Ta and ^{93}Nb quadrupolar nuclei are both ~100% natural abundant, with the predicted ratio of the ^{7}Li−^{93}Nb to ^{7}Li−^{181}Ta dipolar coupling to be ~2, significantly larger than the 10% increase observed experimentally.

Temperature variations in the static and MAS ^{7}Li NMR line shape have been used to detect and describe Li motional dynamics in a variety of materials.[22] The variable temperature (VT) static ^{7}Li NMR spectra for the LiLaNb (pink) material are shown in Figure S1 (in the Supporting Information). There is no significant change in the shape or intensity of the satellite transition (broad component) with temperature, while the central transition shows a gradual decrease in the fwhm with increasing temperature. At the highest elevated temperatures (< 350 K), the central transition begin begins to show a second motionally narrowed Lorentzian component (fwhm ~1000 Hz) but accounts for only ~1% of the total intensity. Similar results were observed for the LiLaNb (tan) material. For the LiLaTa materials, no temperature variations were observed for the satellite transitions (broad component), while analogous to the LiLaNb materials the fwhm of the central transition gradually decreases with increasing temperature. A narrow second component of the central transition (fwhm ~1000 Hz) was observed for all the LiLaTa materials and was present for the entire temperature range investigated, accounting for only ~1.5% of the total intensity with the concentration being invariant to temperature.

Figure 3 and and Figure S1 in the Supporting Information demonstrate that the satellite transition in the static ^{7}Li NMR are visible and invariant over a wide temperature range and that the magnitude of the quadrupolar coupling term does not change significantly between the Ta or Nb materials. The lack of motional averaging on the ^{7}Li satellite transitions shows there are no Li exchange (hopping) processes on the order of the quadrupolar frequency, $\tau \sim \omega_{Q}$(50 kHz). The gradual narrowing of the central transition, combined with only a minor appearance (~1%) of a motionally narrowed Lorentzian component with increasing temperature, show that while there are additional Li dynamics induced by increasing temperature, the correlation times of these motions are on the time-scale of the residual dipolar couplings (~5 kHz). Similar VT ^{7}Li NMR spectra have been reported previously for $Li_5LaNb_{12}O_{12}$ materials.[23] The temperature dependence for this line narrowing ranged from 7 to 15 meV for the different materials. These ^{7}Li NMR line shape results also show that for these different materials there are no large differences in the overall rate of Li dynamics on the 10−100 kHz time scale for the different processed samples. Resolving these differences is complicated by the fact that the Li atom may be located in very different coordination environments as indicated by the ^{6}Li MAS NMR results presented below. Additional information about the Li dynamics can also be

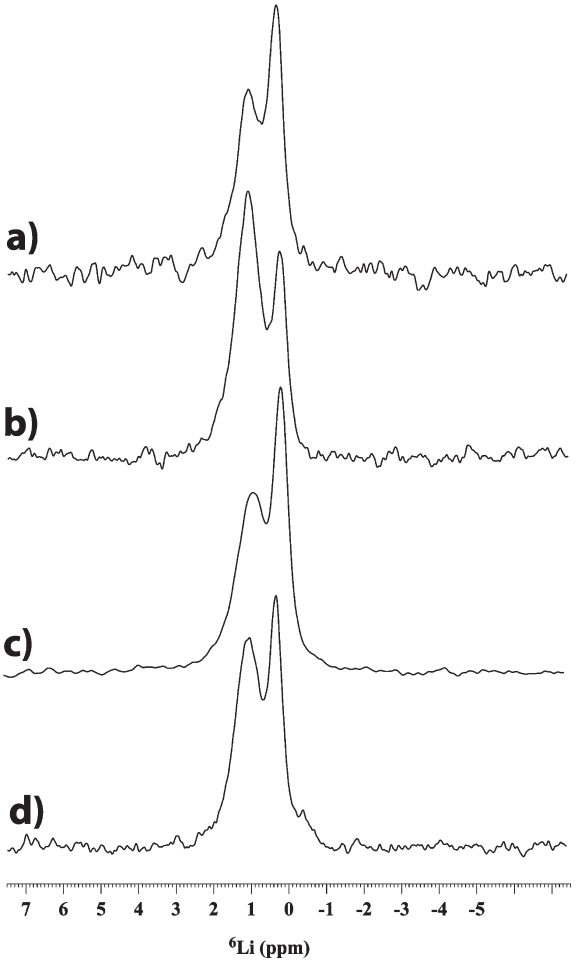

Figure 4. The ^{6}Li MAS NMR spectra for the LiLaTa garnet materials (a) white and (b) tan and the LiLaNb garnet materials (c) pink and (d) tan.

realized by variable temperature spin−lattice relaxation studies, also discussed below.

^{6}Li MAS NMR. The ^{6}Li MAS NMR spectra for the LiLaTa and LiLaNb garnet phases are shown in Figure 4. At this field strength and spinning speed, no spinning sidebands were observed such that the integrated intensities of these resonances reflect the relative concentration of the different Li environments if complete spin−lattice relaxation is realized. In the LiLaTa materials, two dominant resonances are observed at $\delta = +1.1$ ppm and $\delta = \sim+0.3$ to $+0.2$ ppm, while in the LiLaNb materials the dominant resonances are observed at $\delta = +0.9$ and $+0.1$ ppm. Minor unidentified Li environments with increased shielding ($\delta = -0.5$ to -0.6 ppm) were also present in some of the material batches. These resonances are likely impurity phases, present in minimal concentrations so that they are not immediately detectable by powder X-ray diffraction. The chemical shifts, relative concentrations, and fwhm line widths for all the materials are presented in Table 1. These ^{6}Li NMR results clearly demonstrate that there are small changes in the relative amounts of the two dominant Li environments with increased processing.

^{6}Li Peak Assignments. There has been some disagreement with respect to structural models for the garnet phase and identification of lithium environments by both crystallographic techniques and ^{6}Li NMR. In the following section, the possible models are discussed in the framework of assigning ^{6}Li NMR peak positions. In previous ^{6}Li NMR studies of the $Li_5La_3Nb_2O_{12}$ garnet materials,[10] two different Li environments were observed at $\sim +0.7$ and -0.2 ppm ($\Delta\delta = 0.9$ ppm) and were assigned to an octahedral and a tetrahedral Li site, respectively. Their assignment was based on occupancy limits on the tetrahedral sites (60%), ^{6}Li-rotational echo double resonance (REDOR) NMR, along with differential temperature response of the line width for the two different environments.[10] These peak assignments are inconsistent with previous studies that correlate ^{6}Li chemical shifts to structural parameters. Xu and Stebbins predict a more negative NMR chemical shift (higher shielding) with an increased number of bonds to lithium in both amorphous and crystalline lithium silicate materials.[24] Alam et al.[25] reported ^{6}Li chemical shifts for crystalline and amorphous lithium phosphates as a function of a chemical shift parameter (A) based on oxygen-cation bond valences and Li−O bond distances and arrived at a similar conclusion with the more positive chemical shifts corresponding to smaller coordination number. With the use of estimates of the chemical shift parameter A for the current garnet materials, the resonance assignments still remain ambiguous.

Two structural models for $Li_5La_3Ta_2O_{12}$ are worth considering when discussing the ^{6}Li NMR spectra; one based on single-crystal X-ray data[26] and one derived from neutron powder diffraction data.[5] The Li−O bond lengths and bond valence sums for lithium sites are summarized for these two models in Table 2. The lithium sites in $Li_5La_3Ta_2O_{12}$ have generally been described as octahedral or tetrahedral. However, this is not necessarily accurate and subject to where one defines the cutoff Li−O distance to be considered a bond. Instead, we have described in Table 2 each lithium site by its bond valence sum (BVS). A BVS > 1 can generally be described as a Li more tightly bound to its lattice, and a BVS < 1 is described a more loosely bound Li environment. The $I2_13$ model[26] has two lithium sites, both loosely bound to the oxide lattice, and the $Ia\bar{3}d$ model[5] has three lithium sites, one tightly bound, one loosely bound, and one intermediate. Although the latter model has more lithium environments than we observe by ^{6}Li NMR, we cannot rule it out since we do not know if the resonances from the different ^{6}Li environments might overlap. Given this general lack of agreement among characterization data for lithium sites of these garnet phases, we hesitate to assign ^{6}Li chemical shifts to specific lithium coordination environments. Furthermore, there probably exists a range of local coordination environments, both between samples and within a given sample, that differ as a function of both

(24) Xu, Z.; Stebbins, J. F. *Solid State Nucl. Magn. Reson.* **1995**, *5*, 103–112.
(25) Alam, T. M.; Conzone, S.; Brow, R. K.; Boyle, T. J. *J. Non-Cryst. Solids* **1999**, *258*, 140–154.
(26) Hyooma, H.; Hayashi, K. *Mater. Res. Bull.* **1988**, *23*, 1399–1407.

Table 1. ^{6}Li MAS NMR of Garnet Electrolyte Samples

sample name	processing history[a]	$\delta(^6\text{Li})$, ppm (% of spectrum), line width[b]
LiLaTa-white	two steps: 700 °C, then 900 °C	+1.1 (54%), fwhm = 63 Hz +0.3 (46%) fwhm = 25 Hz
LiLaTa-tan	seven steps: 700 °C, then 6× 900 °C; followed by 4 days of continuous heating at 900 °C	+1.1 (75%) fwhm = 64 Hz +0.2 (25%) fwhm = 23 Hz
LiLaNb-pink	three steps: 700 °C, then 2× 900 °C	+0.9 (47%) fwhm = 55 Hz +0.2 (53%) fwhm = 26 Hz
LiLaNb-tan	three steps: 700 °C, then 2× 900 °C, followed by 4 days of continuous heating at 900 °C	+1.1 (65%) fwhm = 46 Hz +0.3(33%) fwhm = 22 Hz −0.4 (2%) fwhm = 20 Hz
LiLaTa-white pH 3 $H^+ \rightarrow Li^+$ exchange/dehydration		+1.0 (85%) fwhm = 47 Hz +0.2(15%) fwhm = 26 Hz
LiLaTa-tan pH 3 $H^+ \rightarrow Li^+$ exchange/dehydration		+1.0 (95%) fwhm = 33 Hz +0.1 (2%) fwhm = 25 Hz −0.6 (3%) fwhm = 37 Hz
LiLaNb-pink pH 3 $H^+ \rightarrow Li^+$ exchange/dehydration	mixing and heating as described above, followed by pH 3 $H^+ \rightarrow Li^+$ exchange/dehydration	+0.9 (80%) fwhm = 50 Hz +0.2 (20%) fwhm = 22 Hz
LiLaNb-tan pH = 3 $H^+ \rightarrow Li^+$ exchange/dehydration		+1.0 (80%) fwhm = 52 Hz +0.2 (15%) fwhm = 30 Hz −0.6 (5%) fwhm = 30 Hz

[a] If heating time not indicated, it is generally 6−9 h. Each heating step is preceded by remixing in an alcohol slurry in the Turbula. Around 10% excess LiOH is usually added for the remixing (see text for details). [b] Full width at half-max, estimated error for ^{6}Li MAS NMR ± 5 Hz. Estimated error in δ is ±0.1 ppm, and in relative concentration ±5abs plot %. All integrals obtained from 600 s direct Bloch decay.

Table 2. Li−O Bond Lengths and BVS[a] for Two Structural Models of $Li_5La_3Ta_2O_{12}$

		$Li_5La_3Ta_2O_{12}$[26]				$Li_5La_3Ta_2O_{12}$[5]	
space group		$I2_13$ (no. 199)				$Ia\bar{3}d$ (no. 230)	
a (Å)		12.804				12.8065	
method		X-ray, single crystal				neutron diffraction, powder	
atom 1 (Li)	atom 2 (O)	bond length (Å)	bond valence sum	atom 1 (Li)	atom 2 (O)	bond length (Å)	bond valence sum
Li1	O3	2.138(9)	**0.799**	Li1	O1	1.936(0)	**1.22**
	O4	2.145(9)			O1	1.936(0)	
	O2	2.148(9)			O1	1.936(0)	
	O3	2.213(9)			O1	1.936(0)	
	O1	2.409(9)		Li2	O1	1.985(10)	**0.878**
	O2	2.805(9)			O1	1.985(10)	
	O3	2.990(9)			O1	2.357(3)	
Li2	O2	2.165(9)	**0.854**		O1	2.357(3)	
	O4	2.177(9)			O1	2.458(9)	
	O1	2.177(9)			O1	2.458(9)	
	O3	2.199(9)		Li3	O1	1.821(6)	**1.02**
	O4	2.230(9)			O1	2.014(11)	
	O1	2.415(9)			O1	2.116(8)	
					O1	2.350(8)	
					O1	2.729(11)	
					O1	2.773(8)	

[a] BVS calculated utilizing Valence.exe (I.D. Brown); $R_o = 1.497$, $B = 0.370$.

oxygen and lithium site defects (vacancies, disorder, displacement, etc.). However, we can definitely say that there are two distinct lithium populations, and they have different dynamic behavior, as revealed by both the ^{6}Li line shape and ^{7}Li NMR relaxation studies described below. Specifically, the low frequency resonance (smaller chemical shift, $\delta \sim +0.2$ ppm, previously assigned as tetrahedral) is considerably less mobile than the high frequency resonance (more positive chemical shift, $\delta \sim +1$ ppm, previously assigned as octahedral), and we have chosen to refer to these positions as tightly bound (nonmobile) lithium and loosely bound (mobile) lithium environments, respectively. It should be noted that the use of mobile and nonmobile is relative to some time scale, and that on the time scale of the ^{7}Li NMR line shape both sites appear as immobile over the temperature range studied. This assignment is also consistent with the observed ^{6}Li NMR T_1s (data not shown), with the low frequency resonance having a much longer T_1 characteristic of a nonmobile (tightly bound) Li environment. In other words, the resonance at $\delta = +1.1$ ppm in the LiLaTa materials) is a loosely bound (mobile lithium), and the resonance at $\delta = +0.2$ to 0.3 ppm is designated as the tightly bound (nonmobile) lithium.

Similarly, in the LiLaNb materials the resonance at $\delta = +0.9$ ppm represent a loosely bound lithium and the resonance at $\delta = +0.1$ ppm is tightly bound lithium. This dynamic difference is consistent with that reported earlier for the garnet $Li_5La_3Nb_2O_{12}$ phase.[10]

For the LiLaTa-white material (Figure 4a), the loosely bound (54%) and tightly bound (46%) lithium are present in similar concentrations. Processing of this material to produce the LiLaTa-pink and LiLaTa-tan samples (Figure 4b) results in the loosely bound site becoming the dominant Li environment (75% tan, Table 1). The initial LiLaNb-pink material showed a similar distribution between the loosely bound (47%) and tightly bound (53%) that was observed in the LiLaTa-white material. Following processing, the LiLaNb-tan material, the loosely bound Li environment, showed a modest increased to 65%.

Since excess LiOH was added at the start of every processing step of the garnet materials, we carried out a series of direct and $^1H-^6Li$ CPMAS NMR experiments to confirm that the majority of the excess LiOH was either being vaporized from the sample during heating or incorporated into the garnet phase. These results are summarized in Figure S3 in the Supporting Information. First, the $^1H-^6Li$ CPMAS NMR spectrum of crystalline $LiOH \cdot H_2O$ shows a single resonance at $\delta = +0.8$ ppm with a line width of 27 Hz. Second, a tantalate sample spiked with $LiOH \cdot H_2O$, in a 2:1 ratio of Li_{garnet}/Li_{LiOH} but not heated to vaporize and/or react the lithium hydroxide with the garnet phase, showed a single CPMAS resonance at +1.1 ppm (Figure S3,top in the Supporting Information). However the direct ^6Li MAS NMR spectrum of this same spiked sample revealed resonances at both +1.1 ppm and +0.1 ppm. It should be noted that there is a small change in the maximum chemical shift between CP and direct, demonstrating that an overlap between the hydroxylated and nonprotonated Li environments in this spiked sample. Finally, a ^6Li CPMAS NMR spectrum of the LiLaTa (white pH $\sim$ 3, $H^+ \rightarrow Li^+$ exchanged, see sample description below) garnet sample that was not spiked with LiOH does not show any signal. These results clearly demonstrate that the $^1H-^6Li$ CPMAS NMR can identify LiOH environments and confirm that there is minimal excess LiOH in the processed samples we have investigated. Therefore, it is also not likely that a significant amount of lithium carbonate or lithium oxide quickly convert to lithium hydroxide in ambient humidity, and lithium carbonate is not stable at the high processing temperatures we utilize. Thus we are confident that the two major ^6Li NMR peaks are characteristic of the garnet oxide lattice rather than an impurity.

The temperature variation of the ^6Li NMR line width for the loosely bound (mobile, octahedral) and tightly bound (nonmobile, tetrahedral) resonances in the LiLaTa (white and tan) and the LiLaNb-pink materials is shown in Figure S2 in the Supporting Information. The unchanged line width of the low frequency (smaller chemical shift) resonance is consistent with the argument that this Li environment is relatively immobile over the temperature range investigated. The temperature variation of the loosely bound site (high chemical shift) is the most significant with an apparent energy of activation (E_a) of 12 meV for LiLaTa-white, 21 meV for LiLaTa-tan, and 18 meV for the LiLaTa-pink samples. The trends in activation energies obtained from these line widths should be treated cautiously for several reasons: (1) The temperature variation was evaluated over a limited range using only 3 data points due to the extensive ^6Li NMR experimental times required due to the long spin−lattice relaxation, and (2) for these samples the dramatic increase in the spectral line width results from spectral broadening due to the interference between the coherent averaging of MAS and the incoherent molecular averaging of Li dynamics[10,27,28] and may not correctly be described by an activation energy . Regardless, the tightly bound (nonmobile) Li environment showed a much smaller temperature variation of the line width ($E_a \sim 0-5.0$ meV) in comparison to the mobile Li resonance for all the samples studied. Again this increased broadening of the ^6Li MAS NMR spectra for the loosely bound (octahedral, mobile) Li resonance is consistent with previous studies on the LiLaNb garnet phase,[10] but for the temperature range investigated our spectra did not show a line width maximum in the fwhm near ambient temperatures as reported in earlier studies.[10] The approximate 2-fold difference in the temperature behavior of the loosely bound (mobile) ^6Li fwhm variation between the LiLaTa-white and the LiLaTa-tan samples provides the first hint that the dynamics in the mobile Li environment can differ based simply on the processing method. This difference between the LiLaTa-white and the LiLaTa-tan samples is further explored in the ^7Li spin−lattice relaxation section below.

^7Li Spin−Lattice Relaxation. To further investigate changes in the high-frequency dynamics of Li following the removal of Li during processing, spin−lattice T_1 relaxation studies on the (1) LiLaTa-white, (2) LiLaTa-tan, and (3) LiLaTa-white that has been pH $\sim$3 adjusted and dehydrated at 600 °C to drive off water (see section on water-treated samples below) while retaining the garnet structure (i.e., see Figure 9). These phases were also chosen because they do not have impurity phases (see Table 1) that might give rise to misleading results. Furthermore, they provide a variation in relative Li-site-occupancy. The spin−lattice relaxation recoveries were fit using the biexponential function detailed in the Experimental Section, with all samples showing bimodal behavior. For the LiLaTa-white material, the long T_1 component dominated (90−95%) over the temperature range studied (298−370 K), while in the LiLaTa-tan sample, the contribution for the long-T_1 component ranges from 37 to 45%. The pH $\sim$ 3 LiLaTa material was also bimodal with the long-T_1 component making between a 20 and 40% contribution. Increased processing appears to reduce the relative fraction of the less mobile long-T_1 dynamical component.

(27) Adolphi, N. L.; Badola, S.; Browder, L. A.; Bowman, R. C. *Phys. Rev., B* **2001**, *65*, 024301.
(28) Suwelack, D.; Rothwell, W. P.; Waugh, J. S. *J. Chem. Phys.* **1980**, *73*, 2559–2569.

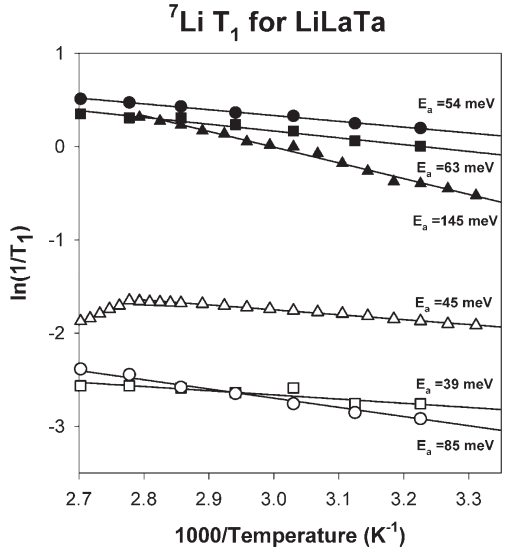

Figure 5. The ^{7}Li spin−lattice T_1 relaxation (long and short T_1 component) as a function of temperature for three samples. LiLaTa (white, ○ = long, ● = short) contains the most lithium and is the result of minimal processing. LiLaTa (tan, □ = long, ■ = short) has lost some lithium due to extensive heating, and LiLaTa (pH∼3, △ = long, ▲ = short) has been Li-depopulated via pH∼3 ion (H^+) exchange followed by dehydration (see text).

The temperature variation of these relaxation times is plotted in Figure 5, assuming the relationship

$$\frac{1}{T_1} \propto \omega_L^{-(1+\beta)} \exp\left(-\frac{E_a}{kT}\right)$$

where ω_L is the Larmor frequency (155 MHz), β is a stretch parameter,[22] and E_a is the activation energy for lithium diffusion. First it should be noted that the highest temperature probed was insufficient to reveal the $1/T_1$ maximum in the LiLaTa-white and LiLaTa-tan samples, while a minimum was observed a $T_1 \sim 5.2$ s for the pH∼3 $H^+ \rightarrow Li^+$ exchange/dehydrated processed sample. This $1/T_1$ maximum occurs when the Li dynamic correlation time is equal to the inverse of the Larmor frequency ($\tau_c \sim 1/\omega_L$) and predicts a correlation time of ∼1 ns for the Li motions responsible for the spin−lattice relaxation. For the other two samples, a maximum in the relaxation was not observed for the temperature range probed, and as such the correlation times were not be determined. The observed Li dynamics are still on the "slow" side of the relaxation curve with increasing temperatures resulting in shorter T_1 relaxation times. Analysis of the temperature dependence for LiLaTa-white gives E_a = 85 meV (long T_1component) and 54 meV (fast T_1 component), for the LiLaTa-tan material an E_a = 39 meV (long T_1 component) and 63 meV (short T_1 component), and in the pH∼3 treated material an E_a = 45 meV (long T_1 component) and 145 meV (short T_1 component) were observed. The pH ∼ 3 $H^+ \rightarrow Li^+$ exchange/dehydration treatment shows a distinct increase in the relaxation rate of the slow component due to decreasing correlation times (the $1/T_1$ maximum was observed in this sample). The fast relaxing component shows a decrease in the relaxation rate in comparison to the fast component of the LiLaTa-tan sample but a higher energy of activation.

It has been argued that the paramagnetic Ta^{+4}/Nb^{4+} centers introduced during the processing may influence the observed relaxation rates. The impact of paramagnetic impurities on ^{7}Li relaxation is well-known and can influence not only the overall rate but the E_a calculated.[29] While we have not directly determined the concentration of these possible paramagnetic centers, we believe they are not responsible for the large changes in relaxation observed between the different processed materials. First, increasing the concentration of paramagnetic centers with increased heat processing should in general increase the observed relaxation rates. This does not appear to be the case in comparison between the LiLaTa-white and the LiLaTa-tan sample where the slow and fast component relaxation times are very similar at room temperature. In addition, we discount the introduction of other external paramagnetic impurities (Fe, Mn) in the processed samples since the same starting materials were utilized in all cases. These select samples show very complex, multicomponent relaxation. The work reported in this paper is not meant to represent an extensive characterization of the Li dynamic in these materials but instead is presented to demonstrate that there are distinct changes that are occurring as a function of processing. A more thorough characterization of the Li dynamics is planned in the future.

Lithium Loss Due to Volatility or $H^+ \rightarrow Li^+$ Exchange of Garnet Materials and Conversion to La_2LiTaO_6 Perovskite. We use infrared spectroscopy as another means of examining the lithium in the garnet electrolyte materials, in addition to documenting the effect of Li-content on phase stability. Figure 6 shows infrared spectra of the three tantalate garnet powders, LiLaTa-white, pink, and tan. There are several distinct peaks that show obvious changes as a function of increased heating time. These are the doublet centered at 1470 and 1430 cm^{-1} and the small peak at 877 cm^{-1}. The doublet is strong and distinct for LiLaTa-white and becomes broader and less distinct for LiLaTa-pink. Finally, for LiLaTa-tan, this peak is much diminished, as is the small peak at 877 cm^{-1}. Additionally, infrared spectra of any powder samples of the Nb or Ta garnet analogues that have been aqueous-treated revealed complete disappearance of these peaks. An example infrared spectrum is shown in Figure 6, for LiLaTa-pink that has been $H^+ \rightarrow Li^+$ exchanged, recollected by filtration, and dried. Aqueous acidification of a garnet sample produces similar infrared spectra. In addition, ^{6,7}Li NMR of the garnet powders stirred in water and adjusted to pH∼3 were also pursued. The room temperature static ^{7}Li NMR spectra (Figure S4 in the Supporting Information) have spectra that are almost identical to the original LiLaTa and LiLaNb materials, consisting of an overlapping broad and narrow component resulting from the satellite and central transitions and reveal no significant differences with the $H^+ \rightarrow Li^+$

(29) Grüne, M.; Müller-Warmuth, W. *Solid State Magnetic Resonance* **1995**, *5*, 145–150.

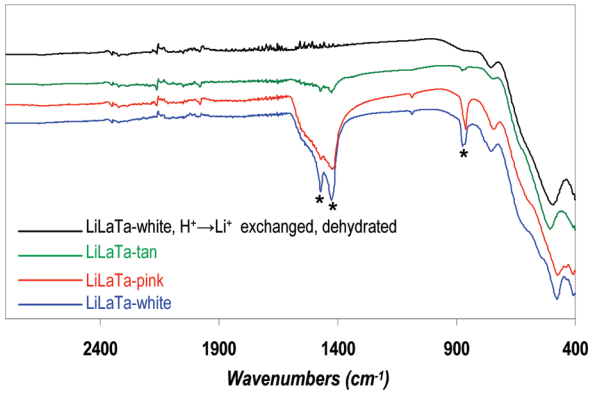

Figure 6. Infrared spectra of garnet powders. The ∗ denote the vibration bands associated with the nonmobile lithium. These peaks broaden and diminish with increasing mixing/heating processing or $H^+ \rightarrow Li^+$ exchange in water.

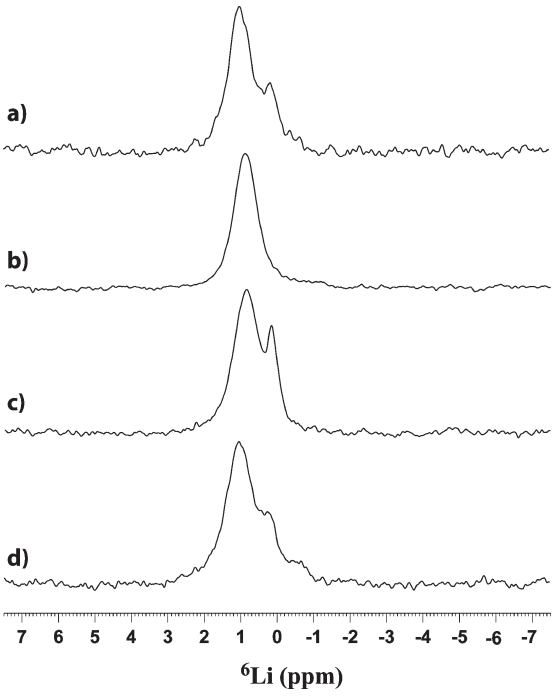

Figure 7. The ^{6}Li MAS NMR spectra for the $H^+ \rightarrow Li^+$ exchanged LiLaTa and LiTaNb (pH ~ 3) materials: (a) LiLaTa-white, (b) LiLaTa-tan, (c) LiLaNb-pink, and (d) LiLaNb-tan.

exchange. The ^{6}Li MAS NMR for the pH~3 treated Ta and Nb garnet materials are shown in Figure 7. These spectra in general show an increased relative concentration of the loosely bound (mobile, octahedral) Li environment (δ = +1.0 ppm, Table 1) following water treatment. The high-speed ^{1}H MAS NMR spectra (data not shown) for these $H^+ \rightarrow Li^+$ exchanged garnet powders shows a major, very broad resonance at δ = +4.7 ppm. The peak position is consistent with prior assignments of −OH in tantalate or niobate frameworks[30] but more than twice the line-width due to exchange between different water environments or variability in coordination site geometry.

The combined IR and lithium NMR data on $H^+ \rightarrow Li^+$ exchanged garnet samples suggests that the lithium in the

(30) Nyman, M.; Rodriguez, M. A.; Alam, T. M.; Anderson, T. M.; Ambrosini, A. *Chem. Mater.* **2009**, *21*, 2201–2208.

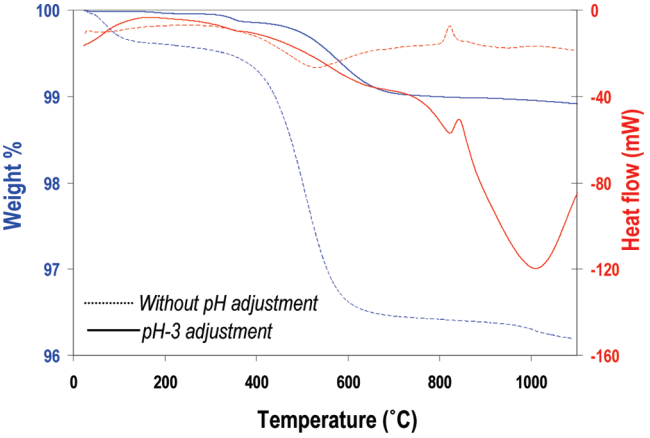

Figure 8. Thermogravimetry-differential scanning calorimetry (TGA-DSC) of LiLaTa-white after pH~3 $H^+ \rightarrow Li^+$ exchange. The solid lines are for ion-exchange without pH adjustment, the dashed lines are for pH 3 ion exchange. The weight loss is exchanged in protons volatilized as H_2O. The exothermic phase change around 850 °C is partial conversion to La_2LiTaO_6.

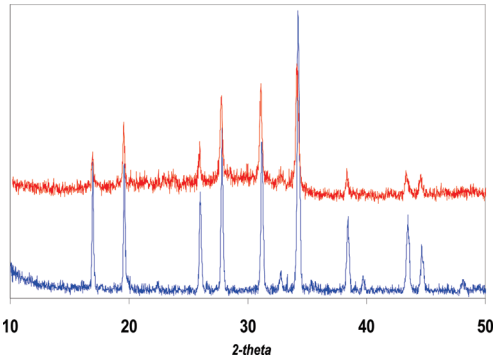

Figure 9. X-ray diffraction spectra of (1) pristine tantalate garnet (blue) and (2) tantalate garnet that has been $H^+ \rightarrow Li^+$ exchanged at pH ~3, followed by dehydration via heating at 600 °C for 1 h. The phase is largely preserved but with some diminishment in crystallinity.

tightly bound, nonmobile sites are being removed by exchange with protons. It appears as if the Li- ions in the nonmobile site undergo $H^+ \rightarrow Li^+$ exchange more readily than the mobile Li ions. By inference to the IR spectra of the highly processed garnet samples (pink and tan), the lithium population is also diminished on the nonmobile site by repeated and extensive heating that results in Li_2O vaporization. Thermogravimetry-differential scanning calorimetry (TGA-DSC) of LiLaTa-white garnet stirred in water without acidification shows a ~1−1.5% weight loss from 200 to 600 °C (Figure 8), with an exothermic phase change at 850 °C. The pH~3 $H^+ \rightarrow Li^+$ exchanged LiLaTa-white has a weight loss of ~3.5%, and its phase change takes place at 825 °C, also shown in Figure 8. The weight loss upon heating occurs as follows:

$$Li_{5-x}H_xLa_3Ta_2O_{12} \rightarrow \Delta \rightarrow x/2(H_2O) + Li_{5-2x}La_3Ta_2O_{12-x}$$

A ~1 wt % loss by TGA corresponds with replacement of ~20% of the Li^+ with H^+ (lost as H_2O), and a 3.5% weight loss corresponds with exchange of ~80% of the Li^+ with H^+. Respectively, these give formulas of Li_4H-$La_3Ta_2O_{12}$ and $LiH_4La_3Ta_2O_{12}$. If the $H^+ \rightarrow Li^+$ exchanged garnet is heated to only 600 °C, the garnet phase

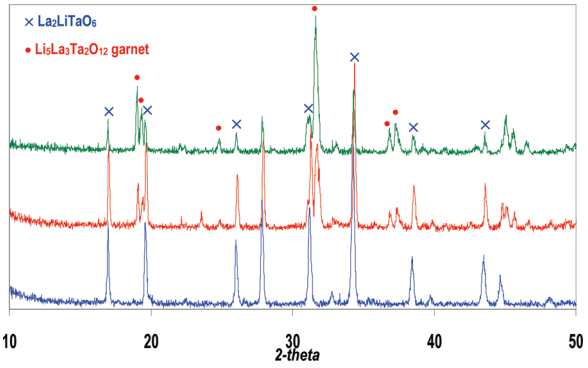

Figure 10. X-ray powder diffraction spectra of (1) pristine tantalate garnet (blue); (2) tantalate garnet $H^+ \rightarrow Li^+$ exchanged in neutral conditions, heated to 1000 °C (red); and (3) tantalate garnet $H^+ \rightarrow Li^+$ exchanged at pH~3, heated to 1000 °C (green). In this series, we observe an increasing loss of the garnet phase, which is replaced by the La_2LiTaO_6 perovskite phase.

remains but with diminished crystallinity. This is illustrated in Figure 9. On the other hand, heating the $H^+ \rightarrow Li^+$ exchanged garnet above 850 °C corresponds with partial or near complete conversion of the garnet phase to the distorted perovskite, La_2LiTaO_6.[31] This is illustrated in Figure 10, where the XRD spectra of (1) the original tantalate garnet, (2) tantalate garnet with $H^+ \rightarrow Li^+$ exchange followed by heating to 1000 °C, and (3) tantalate garnet with a pH~3 $H^+ \rightarrow Li^+$ exchange, followed by heating to 1000 °C. Clearly, the perovskite, La_2LiTaO_6 becomes more prevalent with more lithium removal via $H^+ \rightarrow Li^+$ exchange. Without this $H^+ \rightarrow Li^+$ exchange, the garnet phase is stable at 900 °C indefinitely. However, prolonged heating as a powder without the addition of excess LiOH also results in partial conversion to La_2LiTaO_6. The amount of lithium removed from the garnet after either $H^+ \rightarrow Li^+$ exchange or prolonged heating increases with both the acidity of treatment and/or number of reprocessing steps or excessive heating. By wet chemical analysis such as inductively coupled plasma-mass spectrometry (ICP-MS, Galbraith Laboratories, Inc., Knoxville, TN), the typical pristine tantalate garnet phase has a lithium content of 3.5−4.0% (calculated 3.45%) Tantalate garnet following neutral $H^+ \rightarrow Li^+$ exchange ranges from 2.5 to 2.8% Li (2.65% calculated for ~20% of Li removed). A pH~3 $H^+ \rightarrow Li^+$ exchange results in a garnet phase with ~1% Li (0.86% calculated for ~80% of Li removed). Ranges of Li concentration result from error of the analytical method, perhaps a small amount of excess LiOH or lithium carbonate, and lithium lost as a result of multiple processing steps and/or lengthy heating.

(31) Hayashi, K.; Noguchi, H.; Fujiwara, S. *Mater. Res. Bull.* **1986**, *21*, 289–293.

Summary and Conclusions

This study has shown that decreasing the total lithium population in $Li_5La_3Ta_2O_{12}$ and $Li_5La_3Nb_2O_{12}$ electrolyte powders by taking advantage of lithium oxide volatility results in a decrease of the nonmobile lithium population. Multiple reprocessing by mixing and heating fine powder materials is the protocol for decreasing the lithium content, and we have obtained some samples with only a few percent Li observed in the tightly bound, nonmobile (tetrahedral) environment. Furthermore, as the nonmobile Li-site is depopulated, the remaining Li begins to show changes in the multicomponent ^{7}Li spin−lattice relaxation behavior with the increased appearance of the fast (mobile) environment. Combined infrared studies, thermogravimetry, and ^{6}Li NMR studies have shown that the nonmobile lithium can also be removed preferentially over the mobile lithium via ion-exchange for protons, and the protons are subsequently removed as H_2O by heating to 600 °C, without collapsing the garnet framework. However, at 850 °C these H^+-exchanged materials undergo partial conversion to La_2LiTaO_6 perovskite, the extent of which scales with acidity of the $H^+ \rightarrow Li^+$ exchange.

While prior studies on this family of Li-electrolyte materials have focused on increasing the total lithium population to increase Li-ion mobility (successfully in the case of $Li_6BaLa_2Ta_2O_{12}$), we have taken an alternative approach which has also proved successful. Furthermore, this approach can potentially be evaluated for any metal oxide lithium electrolyte. Probably the most important criteria for improving lithium mobility by depopulating the Li sites via Li_2O volatility or $H^+ \rightarrow Li^+$ exchange/dehydration is a robust framework; that is, it does not collapse or alter to another phase upon the lithium-depopulating processes.

Acknowledgment. We gratefully thank the Laboratory Directed Research and Development (LDRD) program for funding. Sandia is a multiprogram laboratory operated by Sandia Corporation, a Lockheed-Martin Company, for the United States Department of Energy under Contract No. DE-AC04-94AL85000.

Supporting Information Available: File containing additional ^{6}Li and ^{7}Li NMR spectra and data plots (PDF). This material is available free of charge via the Internet at http://pubs.acs.org.